

## Highlights

### **Tree-NET: Enhancing Medical Image Segmentation Through Efficient Low-Level Feature Training**

Orhan Demirci, Bulent Yilmaz

- Bottleneck features contain dense information about data, which is learned by autoencoders.
- These low-level features can be further supervised for segmentation purposes, as they possess the most essential information.
- Tree-NET is a state-of-the-art model framework that uses bottleneck features in both input and output ends that reduces the computational cost when applied to any segmentation model.
- This approach reduces the FLOPs of segmentation models by 4 to 13 times, depending on the architecture, while maintaining comparable accuracy.

# Tree-NET: Enhancing Medical Image Segmentation Through Efficient Low-Level Feature Training

Orhan Demirci<sup>a,b,\*,1</sup>, Bulent Yilmaz<sup>c,\*\*,2</sup>

<sup>a</sup>Electrical and Computer Engineering Department, Abdullah Gul University, , Kayseri, 38080, Türkiye

<sup>b</sup>Computer Engineering Department, Hacettepe University, 06800, Ankara, Türkiye

<sup>c</sup>GUST Engineering and Applied Innovation Research Center (GEAR), Electrical and Computer Engineering Department, Gulf University for Science and Technology (GUST), Hawally, 32093, Kuwait

## ARTICLE INFO

### Keywords:

Autoencoders  
U-NET  
Bottleneck Feature Supervision  
Transformers  
Pyramid Vision Transformers (PVT)  
Medical Image Segmentation  
Tree-NET

## ABSTRACT

This paper introduces Tree-NET, a novel framework for medical image segmentation that leverages bottleneck feature supervision to enhance both segmentation accuracy and computational efficiency. While previous studies have employed bottleneck feature supervision, their applications have largely been limited to the training phase, offering no computational benefits during training or evaluation. To the best of our knowledge, this study is the first to propose a framework that incorporates two additional training phases for segmentation models, utilizing bottleneck features at both input and output stages. This approach significantly improves computational performance by reducing input and output dimensions with a negligible addition to parameter count, without compromising accuracy. Tree-NET features a three-layer architecture comprising Encoder-Net and Decoder-Net, which are autoencoders designed to compress input and label data, respectively, and Bridge-Net, a segmentation framework that supervises the bottleneck features. By focusing on dense, compressed representations, Tree-NET enhances operational efficiency and can be seamlessly integrated into existing segmentation models without altering their internal structures or increasing model size. We evaluate Tree-NET on two critical segmentation tasks—skin lesion and polyp segmentation—using various backbone models, including U-NET, U-NET++, and Polyp-PVT. Experimental results demonstrate that Tree-NET reduces FLOPs by a factor of 4 to 13 and decreases memory usage, while achieving comparable or superior accuracy compared to the original architectures. These findings underscore Tree-NET's potential as a robust and efficient solution for medical image segmentation.

## 1. Introduction

Segmentation of medical images presents significant challenges compared to natural image segmentation due to irregularities in the size, shape, and intensity of target objects, high rates of false positives, and the cost and time required for annotation [1]. These issues are further compounded by the scarcity of annotated datasets and the stringent clinical precision required, as even minor segmentation errors can adversely impact diagnosis and treatment outcomes.

Traditional segmentation models, such as U-NET and variants of U-NET [2, 3] and fully convolutional networks (FCNs) [4], have been the backbone of medical image segmentation. These architectures, built on encoder-decoder designs, utilize skip connections to combine coarse-grained semantic features with fine-grained spatial details, enabling accurate delineation of complex structures. While effective,

these models often struggle with capturing long-range dependencies and generalizing to diverse datasets, particularly when training data is limited.

While numerous segmentation models have been proposed in the literature, few address the bottleneck feature vector, which encapsulates highly condensed information from the input images.


One notable architecture is the Bottleneck Feature Supervised U-NET (BS U-NET), which combines the strengths of U-NET with bottleneck feature supervision of label maps to achieve superior segmentation results [5]. The model comprises two separately trained networks: the Encoding U-NET and the Segmentation U-NET. The Segmentation U-NET is essentially a regular U-NET with an additional loss applied at its bottleneck layer. Here, labels derived from the bottleneck features—extracted from the intermediate layers of the Encoding U-NET, which is basically an autoencoder [6] trained using label data—encapsulate rich, high-level information that can enhance segmentation accuracy and generalizability.

Despite the state-of-the-art design of the BS U-NET, there are significant drawbacks related to the network's size and accuracy.

In the test stage, the BS U-NET features an indirect participation of bottleneck supervision. After the Segmentation U-NET is trained, the Encoding U-NET is removed from the network, leaving only the Segmentation U-NET for evaluation. The bottleneck features from the Encoding U-NET are used solely to provide a supportive loss to the

\*Corresponding author

\*\*Principal corresponding author

 orhandemirci@cs.hacettepe.edu.tr (O. Demirci);

ylmaz.b@gust.edu.kw (B. Yilmaz)

ORCID(s): 0009-0008-2120-915X (O. Demirci); 0000-0003-2954-1217

(B. Yilmaz)

<sup>1</sup>O. Demirci was responsible for the development of the model and the execution of experiments.

<sup>2</sup>B. Yilmaz served as the advisor for this research, providing guidance, review, and administrative oversight.

original U-NET during training, meaning that during testing, the BS U-NET model's structure is identical to the original U-NET structure. Consequently, there is no computational performance increase, and the approach only slightly impacts accuracy.

More recently, transformer-based architectures, such as Pyramid Vision Transformers (PVT) [7], Polyp-PVT [8], TransUNet [9, 10], and Swin UNet [11], have emerged as powerful alternatives in medical image segmentation. Unlike convolutional models, transformers leverage attention mechanisms to capture global contextual information, enabling superior performance on tasks requiring both fine-grained and long-range feature representation. For instance, TransUNet incorporates transformers into its encoder, capturing long-range dependencies while retaining critical spatial details via skip connections. Similarly, Swin UNet employs hierarchical attention mechanisms, improving computational efficiency and performance across diverse datasets. Polyp-PVT, designed specifically for polyp segmentation, excels in delineating irregular and complex boundaries.

Despite their promise, transformer-based models face challenges such as heavy computational demands, substantial memory requirements, and limited interpretability, all of which hinder their clinical applicability [12]. These limitations underscore the pressing need for segmentation models that effectively balance accuracy, efficiency, and generalizability.

One major challenge is the significant computational burden, especially in 3-D tasks like volumetric brain or lung segmentation [13], which leads to increased processing times and substantial demands on hardware resources, making real-time analysis difficult. High-resolution medical images and complex architectures also result in excessive memory consumption, often causing out-of-memory errors. Additionally, achieving high accuracy with transformer-based models typically requires extensive datasets and prolonged training periods, which are compounded by the scarcity and cost of annotated medical images. Transformers' reliance on large datasets for effective training poses a major limitation in the field, where data is often limited. Furthermore, their high parameter counts increase the risk of overfitting, particularly on small datasets, a common scenario in medical imaging.

Generalization is another concern, as models trained on specific datasets often perform poorly when applied to different medical imaging contexts due to variations in imaging techniques, patient populations, and disease presentations [12]. Biases present in training data can further reduce their reliability across diverse clinical applications. Interpretability remains a critical issue, as understanding the decisions of transformer models is essential for clinical validation and trust. Lastly, their integration into clinical workflows is challenging, as their outputs frequently require adaptation to meet specific clinical requirements.

To address these issues, Tree-NET, a novel state-of-the-art architecture is presented for segmentation issues based on bottleneck feature supervision of both input and label

masks and then creating a bridge network between them to train their low-level representations (Figure 1). The network consists of three main components named Encoder-Net, Decoder-Net and Bridge-Net as each having separate training processes. After the trainings of each component are completed, all three components are combined end-to-end and available for the segmentation task. By this technique, the bridge network of choice is trained with smaller sized input and label images without losing any essential features improving the model performance in terms of accuracy and computational cost while keeping the trainable parameters almost the same number.

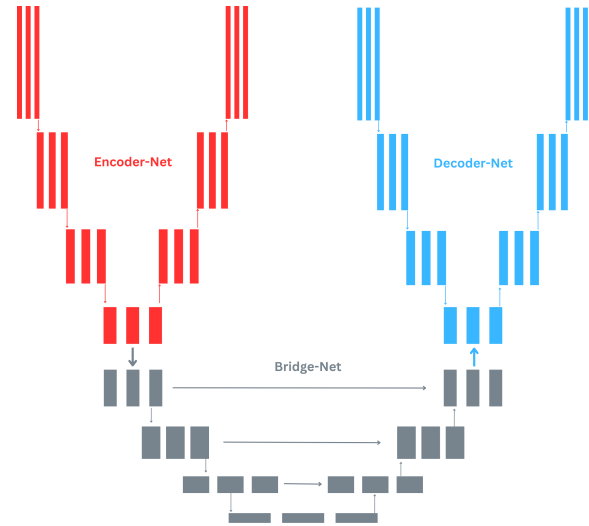


**Figure 1:** General Tree-NET diagram. Red blocks denote the Encoder-Net for input encoding. Gray blocks represent the U-NET architecture as the Bridge-Net for segmentation training. Blue blocks indicate the Decoder-Net for output decoding to match the original label size.

In this study, we introduce Tree-NET, a novel deep learning architecture with a unique autoencoder-supported design that significantly enhances segmentation performance while reducing computational costs. Our key contributions are as follows:

- We propose Tree-NET, a deep learning model that employs bottleneck feature supervision to refine segmentation training. This architecture leverages the low-level representations of input and label data to improve segmentation outcomes.
- Tree-NET features an end-to-end structure composed of three distinct components—Encoder-Net, Bridge-Net, and Decoder-Net. Each component undergoes isolated training before integration, optimizing feature learning and model performance.
- The model utilizes Encoder-Net and Decoder-Net to supervise input and label data, respectively, before the segmentation training conducted by Bridge-Net. This approach enhances feature learning by allowing for more learning steps and a more coordinated

architecture. Additionally, it provides the flexibility to use different hyperparameters for each component, optimizing performance.

- Bridge-Net, a key component of Tree-NET, can be implemented using various existing segmentation algorithms. This flexibility allows Tree-NET to adapt to different segmentation methods and requirements, making it a versatile tool for various applications.
- Tree-NET reduces computational costs by shrinking input and label sizes without loss of critical information. This results in decreased memory usage and improved processing speed, all while enhancing segmentation accuracy.

## 2. Model Architecture

The Tree-NET model consists of three main components such as Encoder-Net, Bridge-Net, and Decoder-Net.

### 2.1. Encoder-Net

Encoder-Net is a convolutional autoencoder model consisting of encoder and decoder parts (see Figure 2).

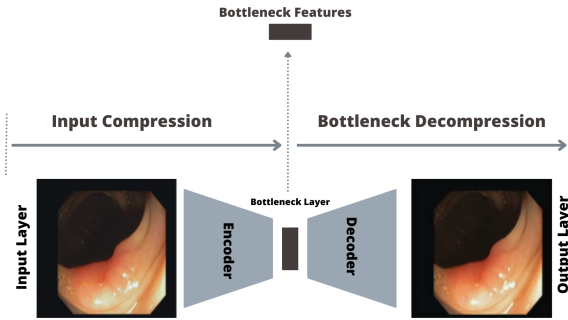


Figure 2: Schematic representation of Encoder-Net.

It is designed to extract low-level representations (bottleneck features) from input images. During training, the Encoder-Net processes the input images to generate these bottleneck features, which are then fed into the Bridge-Net for segmentation training. This means that, once training is complete, only the encoder part of the Encoder-Net is used. (See Figure 5)).

### 2.2. Bridge-Net

As the name implies, Bridge-Net is the network where the Encoder-Net and Decoder-Net are integrated. In this model, the bottleneck features from the Encoder-Net are fed into the Bridge-Net while the bottleneck features of Decoder-Net are used as the labels. Figure 3 explains the process. Bridge-Net is a framework that any type of segmentation model can be used for this purpose. In our experiment, we use U-Net, U-Net++ and Polyp-PVT as the Backbone (BB) models for the Bridge-Net in segmentation tasks.

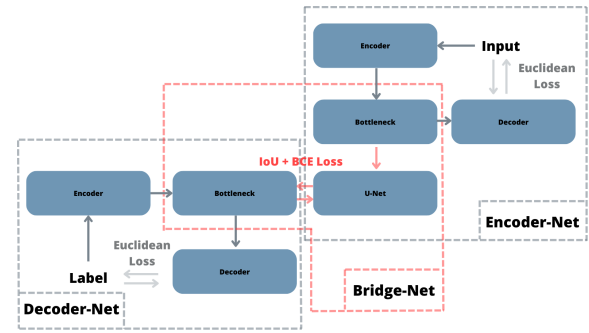


Figure 3: Tree-NET Components: The diagram illustrates the Encoder-Net, Bridge-Net, and Decoder-Net. Unidirectional arrows indicate the data flow through the networks, while bidirectional arrows represent the process of loss computation.

### 2.3. Decoder-Net

Decoder-Net has a similar structure with the Encoder-Net. The main difference is that it extracts the low-level representation (bottleneck feature) of labels masks. The Decoder-Net training is separately applied on label images and bottleneck features obtained for training the Bridge-Net (Figure 4). After training is complete, only the decoder part of the Decoder-Net is used to convert the output back to its original size, producing the final segmentation result. (See Figure 5)).

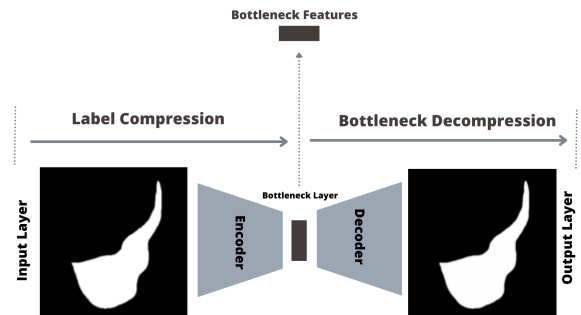


Figure 4: Schematic representation of Decoder-Net.

### 2.4. Overall Architecture

By integrating the three trained components—Encoder-Net, Bridge-Net, and Decoder-Net—the Tree-NET model is constructed for evaluation and practical application. During this integration, the decoder component of the Encoder-Net and the encoder component of the Decoder-Net are removed, as they are only necessary for the training phase. Figure 5 represents the assembled architecture of the Tree-NET.

## 3. Experiments

### 3.1. Dataset Descriptions

There are two main datasets used to evaluate the proposed architecture’s performance such as colon polyps on colonoscopy images and skin cancer on dermoscopic images.

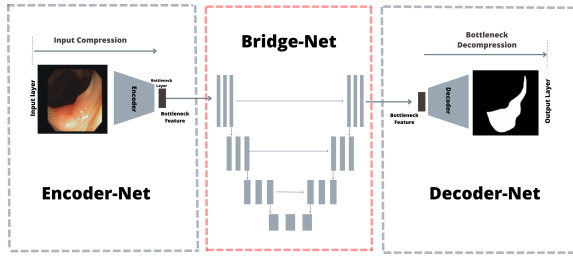


**Figure 5:** Tree-NET diagram. The Encoder part of the Encoder-Net, Bridge-Net, and Decoder part of the Decoder-Net are assembled end-to-end, forming the overall structure.

### 3.1.1. CVC-ClinicDB Dataset

The CVC-ClinicDB dataset [14], developed by the Computer Vision Center (CVC), is a comprehensive resource designed to advance the field of colonoscopy image analysis through the development and benchmarking of automated diagnostic algorithms. This dataset supports several primary tasks: polyp detection, polyp segmentation, and colonoscopy image classification. CVC-ClinicDB is the official database designated for use in the training stages of the MICCAI 2015 Sub-Challenge on Automatic Polyp Detection Challenge in Colonoscopy Videos.

The dataset includes 612 original images with corresponding segmentation ground truths, each representing regions covered by polyps. The images have a resolution of  $384 \times 288 \times 3$ . For our purposes, the dataset will be used exclusively for segmentation. Figure 6 shows sample polyp images along with their segmentation ground truths from the CVC-ClinicDB dataset.

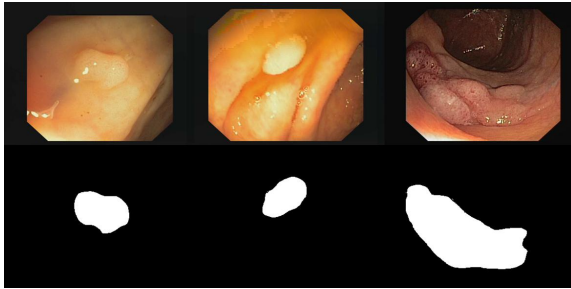


**Figure 6:** Sample polyp images (upper row) and segmentation ground truths corresponding to the regions covered by polyps (lower row).

### 3.1.2. ISIC-2018 Dataset

The ISIC-2018 dataset [15, 16], developed by the International Skin Imaging Collaboration (ISIC), is a comprehensive resource designed to advance the field of skin lesion analysis through the development and benchmarking of automated diagnostic algorithms. This dataset supports three primary tasks: lesion segmentation, lesion attribute detection, and disease classification.

The dataset comprises 2,594 high-resolution dermoscopic images ( $1022 \times 767$  pixels) for training, 100 images for validation, and 1,000 images for testing. Each original

image is accompanied by corresponding ground truth masks that delineate the boundaries of the lesions. For our purposes, the dataset will be used exclusively for segmentation. Figure 7 shows sample skin lesion images along with their segmentation ground truths from the ISIC-2018 dataset.

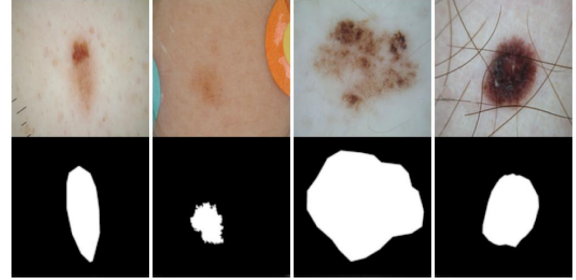


**Figure 7:** Original skin lesion samples (upper row) and corresponding ground truth masks (lower row).

## 3.2. Preprocessing

The four main parts of the preprocessing in order are as follows. Datasets are resized into  $384 \times 384 \times 3$ . For CVC-ClinicDB, with respect to the length of dataset input 612, a randomized index is created, and index values are saved to shuffle the data for training all three components such as Encoder-Net, Bridge-Net and Decoder-Net (the identical index is applied for the other algorithms) to keep the same experiment. For CVC-ClinicDB, the dataset is divided into three parts such as training, validation and test with the ratios of 0.8, 0.1, and 0.1 respectively. For the ISIC-2018, the data is split into training, validation and test parts by default. Inputs and labels in the datasets are normalized into 0 and 1.

## 3.3. Training Procedure

To complete the training of Tree-NET, Encoder-Net and Decoder-Net are trained initially. Then the input is fed into the Encoder-Net, and bottleneck features are collected to create the new input data with size of  $3 \times 96 \times 96$ . The same process is also applied to label data using Decoder-Net and label data with size  $3 \times 96 \times 96$  is obtained. For the Polyp-PVT, label data is shrunk into the  $16 \times 24 \times 24$  to remove its internal step of upsampling and doing it in Decoder-Net instead. The selection model of Bridge-Net as U-NET, U-NET++ and Polyp-PVT are fed with the created inputs and supervised by the created labels. When these three training processes are completed, encoder part of the Encoder-Net, the Bridge-Net and decoder part of the Decoder-Nets are assembled end-to-end respectively.

In training, the dataset is fed through the network through 3 various sizes called as a multi-scale training strategy [17, 18]. The hyperparameter configuration is as follows: the AdamW [19] optimizer, commonly used in transformer networks [7, 20, 21], is utilized for updating the network parameters. Both the learning rate and weight decay are set to  $1 \times 10^{-4}$ . During training, input images are resized to  $352 \times 352$ , with a mini-batch size of 8, over 100 epochs.

**Table 1**

Training parameters. Tree-NET denotes the integrated architecture comprising Encoder-Net, Decoder-Net, and Bridge-Net.  $N$  denotes the spatial dimensions (height and width) of the input image,  $B$  represents the number of feature maps at the bottleneck layer, and  $L$  denotes the spatial dimensions of the bottleneck feature map.  $E$  and  $D$  indicate the feature depths at the bottleneck layers of the encoder and decoder, respectively.  $e$  and  $d$  indicate the spatial dimension reduction ratio at the encoder and decoder, respectively.

	Encoder-Net	Bridge-Net	Decoder-Net
Input Size	$3 \times N \times N$	$3 \times (N/e) \times (N/e)$	$3 \times N \times N$
Bottleneck Size	$3 \times (N/e) \times (N/e)$	$B \times L \times L$	$D \times (N/d) \times (N/d)$
Output Size	$3 \times N \times N$	$D \times (N/d) \times (N/d)$	$1 \times N \times N$
Random Seed	42	42	42
Batch Size	8	8	8
Learning Rate	0.001	0.0001	0.001
Loss Function	Euclidean	wIoU + wBCE	Euclidean
Optimizer	AdamW	AdamW	AdamW
Epoch Number	100	100	100

### 3.4. Parameters

For the segmentation networks such as Bridge-Net, U-NET, U-NET++, BS U-NET, and Polyp-PVT most of the hyperparameters are kept the same such as the optimizer type, batch size and the learning rate in order to keep the experimental setup the same. For the Encoder-Net and Decoder-Net, due to the smaller number of hyperparameters and different structures, the optimum values vary from the segmentation networks. Thus, they are selected separately as shown in Table 1. The Bridge-Net is trained using different segmentation model backbones which are also used as our comparison models. All the comparison models such as U-NET, U-NET++ and Polyp-PVT are trained the same way as the Bridge-Net.

For U-NET, U-NET++, and Polyp-PVT models, combinations of weighted Intersection over Union (IoU) loss [22] and weighted Binary Cross-Entropy (BCE) loss [22] are utilized. The IoU loss mitigates the issue of class imbalance by focusing on the overlap between predicted and ground truth segments, while the BCE loss ensures pixel-wise accuracy [23]. The total loss for these models can be expressed as:

$$\mathcal{L} = \mathcal{L}_{wIoU} + \mathcal{L}_{wBCE} \quad (1)$$

In this equation,  $\mathcal{L}_{wIoU}(\cdot)$  represents the weighted Intersection over Union (IoU) loss, and  $\mathcal{L}_{wBCE}(\cdot)$  denotes the weighted Binary Cross-Entropy (BCE) loss. Unlike conventional BCE loss, which assigns equal importance to all pixels,  $\mathcal{L}_{wBCE}(\cdot)$  prioritizes difficult pixels by assigning them higher weights, improving the model's ability to capture intricate details in segmentation. Similarly,  $\mathcal{L}_{wIoU}(\cdot)$  extends the standard IoU loss by focusing more on challenging pixels, enabling the model to handle complex structures more effectively.

### 3.5. Evaluation Metrics

For testing, images are resized to  $384 \times 384$ , and no additional post-processing or optimization strategies are applied. The proposed model has been evaluated and compared with the other models in terms of accuracy and computational performances.

#### 3.5.1. Accuracy Performance

For the accuracy evaluation, we utilize the Dice coefficient [24], Intersection-Over-Union (IoU) [25], and accuracy (ACC) scores on the test dataset. They are calculated with the true positive (tp), true negative (tn), false positive (fp), false negative (fn) values [26]. These metrics provide a comprehensive assessment of the segmentation quality, capturing various aspects of the model's performance.

The Dice coefficient, also known as the Dice Similarity Coefficient (DSC), measures the overlap between the predicted segmentation and the ground truth. It is particularly useful in medical image segmentation due to its sensitivity to both false positives and false negatives. The Dice coefficient is defined as:

$$\text{Dice Coefficient} = \frac{2 \cdot tp}{2 \cdot tp + fp + fn} \quad (2)$$

The IoU quantifies the intersection ratio to the union of the predicted and ground truth masks. It yields a clear indication of the accuracy of the segmentation by measuring the fraction of correctly predicted pixels out of the total pixels in either the prediction or the ground truth. The IoU is calculated as:

$$\text{IoU} = \frac{tp}{tp + fp + fn} \quad (3)$$

Accuracy measures the proportion of correctly classified pixels (both true positives and true negatives) out of the total number of pixels. While accuracy is a straightforward metric, it may not be as informative in cases of class imbalance, which is common in medical image segmentation. Accuracy is given by:

$$\text{Accuracy Score} = \frac{tp + tn}{tp + tn + fp + fn} \quad (4)$$

#### 3.5.2. Computational Performance

The computational performance of the proposed segmentation model was evaluated using metrics such as computational complexity, parameter counts, and memory usage. These analyses provide a comprehensive understanding of the model's efficiency and its suitability for real-world applications.

**Computational Complexity** The computational complexity of the model was assessed using FLOPs (floating-point operations), which measure the total number of operations required to process a single batch. FLOPs were expressed in billions of operations (GFLOPs) to facilitate comparison and provide insights into the computational demands of the model.

**Memory Footprint and Parameter Size** The memory footprint and parameter size of the model were analyzed to assess its resource efficiency. The following metrics were considered:

- **Parameter Counts:** Representing the total number of trainable parameters, measured in millions (M).
- **Peak Memory Usage:** Measuring the maximum memory allocated during computation, expressed in gigabytes (GB).

## 4. Results and Discussion

### 4.1. Encoder-Net & Decoder-Net Results

Figures 8 and 9 illustrate the output results from Encoder-Net and Decoder-Net compared with their ground truths. As it can be seen from visualized results of the Encoder-Net, the output is even clearer than the original input meaning that the autoencoder did not lose much of features from the original input and auto-handled the contrast of the images while shrinking the input size 16 times.

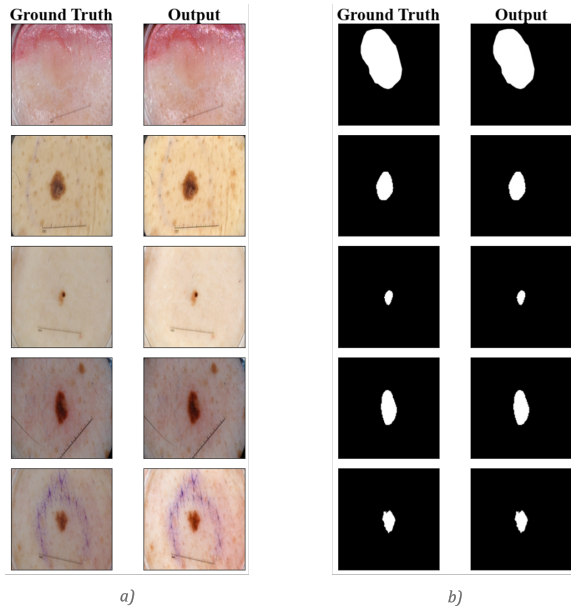


**Figure 8:** ISIC sample test outputs versus ground truth of (a) Encoder-Net and (b) Decoder-Net.

### 4.2. Tree-NET vs Other Models

The performance of the algorithms is compared with traditional methods in terms of accuracy and computational efficiency.

#### 4.2.1. Accuracy Results

The results of the proposed network are compared with other methods such as BS U-NET, U-NET, U-NET++ and Polyp-PVT. The comparisons are visualized in Figure 10. This figure displays samples from the first 5 images selected from the test dataset, which were processed using the aforementioned models. The IoU, Dice, and accuracy scores for the proposed model and the comparison models are detailed in Table 2.

As demonstrated in the figures and table, our design surpasses the others in all metrics, showcasing superior performance across the board.

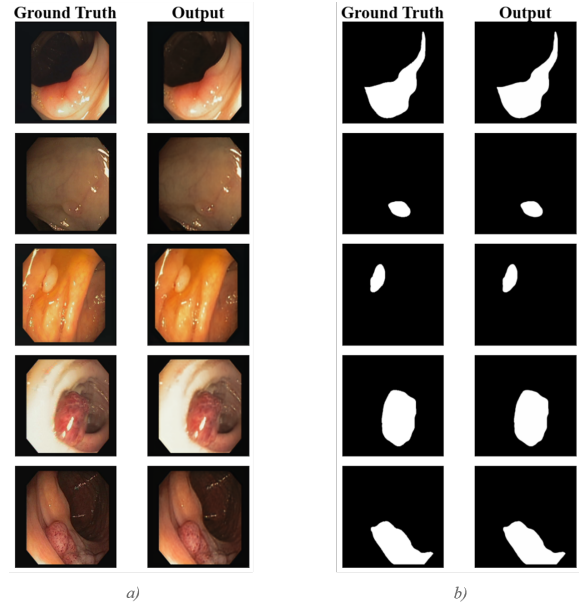


**Figure 9:** CVC-ClinicDB sample test outputs versus ground truth of (a) Encoder-Net and (b) Decoder-Net.

**Table 2**

Performance comparison of the proposed network (Tree-NET) against BS U-NET, U-NET, and U-NET++ in terms of IoU, Dice, and accuracy scores.

Comparison Models		ISIC-2018			CVC-ClinicDB		
		Dice	IoU	Acc	Dice	IoU	Acc
Comparison Models	U-NET	0.807	0.7	0.915	0.936	0.891	0.991
	BS U-NET	0.822	0.723	0.908	0.928	0.883	0.989
	U-NET++	0.829	0.736	0.905	0.94	0.893	0.991
	Polyp-PVT	<b>0.903</b>	<b>0.839</b>	<b>0.944</b>	<b>0.959</b>	<b>0.924</b>	<b>0.994</b>
Tree-NET	U-NET++ BB	0.867	0.79	0.925	0.923	0.872	0.99
	U-NET++ BB	0.862	0.787	0.923	0.9189	0.867	0.989
	Polyp-PVT BB	0.886	0.811	0.935	0.946	0.9	0.992

The results presented in the table demonstrate that our proposed model outperforms the comparison methods across all metrics, exhibiting superior performance overall.

#### 4.2.2. Computational Efficiency

The computational efficiency of the proposed segmentation model was evaluated using FLOPs (floating-point operations), parameter counts, and peak memory usage. These metrics provide a comprehensive understanding of the computational demands and efficiency of each model variant.

The results, summarized in Table 3, include:

FLOPs, which measure the computational complexity of processing a single batch, expressed in billions of operations (GFLOPs). Parameter Counts, representing the total number of trainable parameters in millions (M). Peak Memory Usage, indicating the maximum memory allocated during computation, expressed in gigabytes (GB). The performance of the proposed Tree-NET model was compared against U-NET, BS U-NET, and U-NET++ across different batch sizes. These comparisons reveal that Tree-NET consistently achieves a favorable balance between computational cost and memory efficiency.

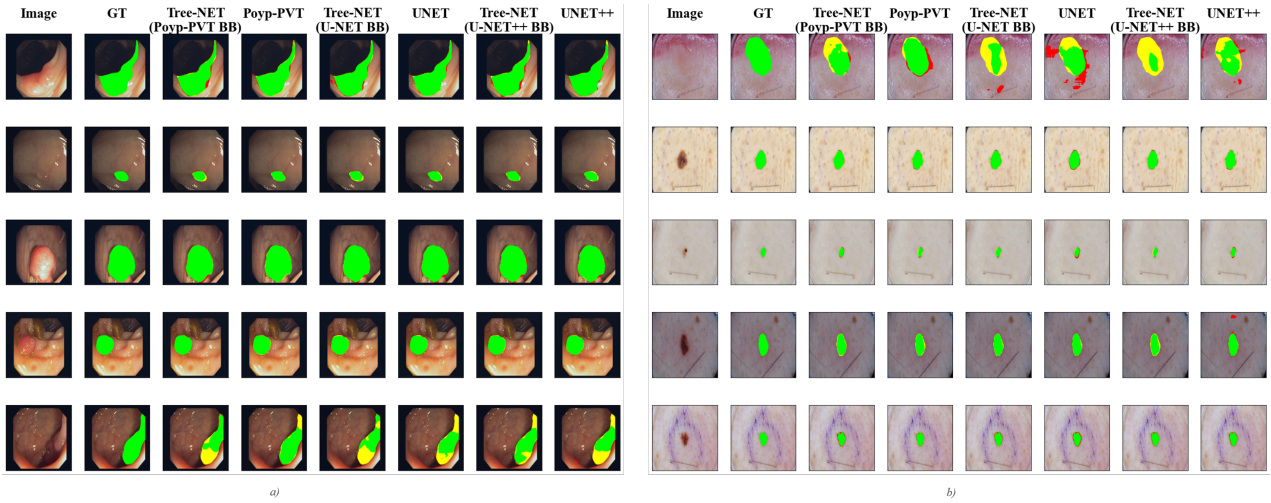


**Figure 10:** Visualization of segmentation results on (a) CVC-ClinicDB and (b) ISIC-2018 test samples, comparing the proposed Tree-NET framework with BS U-NET, U-NET, U-NET++, and Polyp-PVT. Green regions indicate correctly segmented polyps, yellow regions represent missed polyps, and red regions denote incorrect predictions. The input is labeled as "Image," and "GT" represents the Ground Truth.

**Table 3**

Comparative results of the proposed network (Tree-NET) against BS U-NET, U-NET, U-NET++, and Polyp-PVT for computational performance, parameters, and memory usage across different batch sizes.

Model	Variant	Batch	FLOPs (GFLOP)	Parameters (M)	Peak Memory Allocated (GB)
Poyp-PVT BB	Tree-NET	Batch1	2.54	25.17	1.402
		Batch8	20.32	25.17	1.559
	Original	Batch1	11.92	25.11	1.44
		Batch8	95.38	25.11	5.344
	Tree-NET	Batch1	2.85	7.88	1.081
		Batch8	22.77	7.88	4.891
U-NET	BS U-NET	Batch1	33.58	7.88	1.976
		Batch8	268.62	7.88	5.548
	Original	Batch1	31.73	7.85	4.386
		Batch8	253.81	7.85	4.235
	Tree-NET	Batch1	5.77	9.19	1.322
		Batch8	46.18	9.19	1.468
U-NET++	Batch1	78.53	9.16	2.516	
	Batch8	628.26	9.16	8.877	

The results highlight that Tree-NET models exhibit significantly lower computational demands (FLOPs) and memory usage while maintaining a comparable or superior number of parameters. This efficient utilization of resources makes Tree-NET particularly well-suited for practical deployment, where minimizing hardware and energy requirements is critical.

### 4.3. Discussion

Our proposed segmentation model, Tree-NET, demonstrates superior efficiency performance with comparable accuracy results, making it highly advantageous for real-life applications. A critical factor contributing to its efficiency is the superior computational performance in terms of FLOPs and memory footprint.

One of the key strengths of Tree-NET is its ability to achieve significant reductions in FLOPs and memory usage without increasing model size or architectural complexity. This characteristic makes Tree-NET highly adaptable and efficient for integration into existing segmentation frameworks.

The experimental results demonstrate that Tree-NET reduces FLOPs by a factor of 4 to 13 compared with the

original models using the same backbones. For example, with the U-NET backbone and batch size of 1, Tree-NET requires only 2.85 GFLOPs, whereas BS U-NET requires 33.58 GFLOPs. A similar reduction ratio is observed when comparing Tree-NET to the original U-NET model, as BS U-NET is constructed in a similar way.

In terms of memory allocation, Tree-NET consistently outperforms the comparison models by using significantly less memory. This efficiency is achieved through effective low-level representation, where smaller inputs are processed with convolution operations, leading to a substantial reduction in computational load while maintaining comparable accuracy.

To illustrate, feeding inputs of sizes  $(3 \times 384 \times 384)$  and  $(3 \times 96 \times 96)$  into the same model dramatically reduces the number of computations required, even if the number of parameters remains constant. This reduction is due to the computational complexity of convolution operations being directly related to input size. By efficiently handling smaller inputs through low-level representations, our model reduces the overall number of operations, leading to faster processing times and lower energy consumption.

Additionally, the architecture of our model, with its Encoder-Net and Decoder-Net components, is designed to be lightweight yet powerful. Each of these nets has approximately 50,000 trainable parameters, which is relatively low compared to the Bridge-Net used and other state-of-the-art models. Despite this compactness, the performance of our model remains unaffected, demonstrating that it can achieve high segmentation accuracy with fewer resources.

Despite the accuracy and computational performance superiority of the Tree-NET model compared with other approaches, several limitations and challenges in the implementation of the algorithm need to be addressed for it to reach its full potential.



One significant limitation in our comparative testing environment is the absence of pre-trained models for the novel Tree-NET approach. Established algorithms, such as U-NET and U-NET++, often benefit from extensive pre-training on large datasets, facilitating fine-tuning and evaluation. This disparity poses a challenge for a direct performance comparison. For instance, the U-NET model, fine-tuned using the ISIC-2018 dataset, achieved a Dice score of 0.8674 and an Intersection over Union (IoU) score of 0.8491. In contrast, our implementation of the original U-NET, without fine-tuning, yielded a Dice score of 0.807 and an IoU score of 0.7. Similarly, the U-NET++ model, fine-tuned with the same dataset, reached a Dice score of 0.8822 and an IoU score of 0.8651, whereas our non-fine-tuned U-NET++ achieved a Dice score of 0.829 and an IoU score of 0.736 [27].

Integrating Tree-NET into transformer models was challenging. While pre-trained Polyp-PVT was used for integration, the mismatch in model architecture and pre-training strategies resulted in slightly lower performance than the original model. Optimized pre-training strategies for Tree-NET could address this limitation and enhance performance.

These results underscore the performance gains attributable to fine-tuning with a large, relevant dataset. Consequently, it is reasonable to infer that Tree-NET could also achieve superior performance with pre-trained models once they become available. This limitation highlights the necessity for developing and utilizing pre-trained models to enhance the comparative evaluation of novel algorithms.

Another challenge is the meticulous tuning of component parameters and layers within the Tree-NET model. Both the Encoder-Net and Bridge-Net components are designed to progressively shrink the input size to create a compact representation. However, this aggressive downsizing can lead to an overly small bottleneck in the Bridge-Net, potentially rendering many learning parameters ineffective. Striking the right balance in the downsizing process is crucial. If autoencoders are designed with less downsizing, the model may suffer from worse performance due to an inability to effectively capture and compress the essential features of the input data. Conversely, excessive downsizing can lead to information loss and a subsequent drop in segmentation accuracy. This delicate balance requires careful parameter tuning and extensive experimentation to optimize model performance without compromising the integrity of the learned features.

The inherent complexity of the Tree-NET algorithm presents another significant challenge. The model's architecture involves multiple interdependent components, including the Encoder-Net, Bridge-Net, and Decoder-Net, each contributing to the overall performance. Introducing changes or improvements in one component often necessitates corresponding adjustments in the other components to maintain coherence and functionality. This interdependency increases the difficulty of model design and optimization, as each modification must be carefully evaluated to ensure it does

not adversely affect the overall system. Moreover, the complexity of the algorithm may lead to longer training times depending on the design of components.

Another challenge is utilizing various approaches and models as the Bridge-Net component of our Tree-NET architecture. Applying a range of algorithms, particularly larger models, is computationally intensive and time-consuming. In the ISIC-2018 Lesion Boundary Segmentation Challenge, models like Mask RCNN, ensembled models, GANs, and U-NET variants demonstrated the highest IoU scores [28, 29, 30, 31, 32]. Among these, the hybrid Mask RCNN and segmentation model, inspired by DeepLab and PSPNet, achieved the highest IoU score of 0.802. In our experiments, Tree-NET surpassed U-NET and U-NET++ results but showed slightly lower performance compared to Polyp-PVT. However, this comparison is not entirely equitable due to the additional Mask-RCNN boundary detection in the hybrid model. For a more accurate assessment, Tree-NET should incorporate a similar backbone and leverage Mask-RCNN boundary detection.

## 5. Conclusions and Future Prospects

Tree-NET represents a significant advancement in medical image segmentation, offering a robust and efficient solution for tasks like polyp and skin lesion segmentation. By leveraging bottleneck feature supervision, Tree-NET achieves substantial reductions in computational cost and memory usage while maintaining comparable or superior accuracy to state-of-the-art models like U-NET, BS U-NET, and U-NET++.

A standout feature of Tree-NET is its versatility, enabling seamless integration with existing segmentation frameworks across various applications. The architecture's adaptability, particularly through the Bridge-Net, allows for significant computational savings without altering the internal structure of backbone models. This versatility makes Tree-NET a valuable tool for a range of applications beyond medical imaging.

Future work will focus on integrating Tree-NET with alternative backbones, such as FCN, DeepLab, and advanced transformer architectures, to improve performance and scalability. Additionally, pre-training all Tree-NET components could significantly enhance its accuracy and efficiency. These developments will open new opportunities for Tree-NET in areas like medical imaging, remote sensing, and computer vision.

In summary, Tree-NET's innovative design, computational efficiency, and adaptability position it as a groundbreaking framework for advancing image segmentation technologies.

## CRedit authorship contribution statement

**Orhan Demirci:** Conceptualization of this study, Methodology, Software. **Bulent Yilmaz:** Validation, review & editing, Project administration.

## References

- [1] R. Zhao, B. Qian, X. Zhang, Y. Li, R. Wei, Y. Liu, and Y. Pan, "Rethinking dice loss for medical image segmentation," in *2020 IEEE International Conference on Data Mining (ICDM)*. IEEE, 2020, pp. 851–860.
- [2] O. Ronneberger, P. Fischer, and T. Brox, "U-net: Convolutional networks for biomedical image segmentation," in *Medical image computing and computer-assisted intervention—MICCAI 2015: 18th international conference, Munich, Germany, October 5-9, 2015, proceedings, part III 18*. Springer, 2015, pp. 234–241.
- [3] Z. Zhou, M. M. Rahman Siddiquee, N. Tajbakhsh, and J. Liang, "Unet++: A nested u-net architecture for medical image segmentation," in *Deep Learning in Medical Image Analysis and Multimodal Learning for Clinical Decision Support: 4th International Workshop, DLMIA 2018, and 8th International Workshop, ML-CDS 2018, Held in Conjunction with MICCAI 2018, Granada, Spain, September 20, 2018, Proceedings 4*. Springer, 2018, pp. 3–11.
- [4] J. Ji, X. Lu, M. Luo, M. Yin, Q. Miao, and X. Liu, "Parallel fully convolutional network for semantic segmentation," *IEEE Access*, vol. 9, pp. 673–682, 2020.
- [5] L. Song, K. Geoffrey, and H. Kaijian, "Bottleneck feature supervised u-net for pixel-wise liver and tumor segmentation," *Expert Systems with Applications*, vol. 145, p. 113131, 2020.
- [6] K. Berahmand, F. Daneshfar, E. S. Salehi, Y. Li, and Y. Xu, "Autoencoders and their applications in machine learning: a survey," *Artificial Intelligence Review*, vol. 57, no. 2, p. 28, 2024.
- [7] W. Wang, E. Xie, X. Li, D.-P. Fan, K. Song, D. Liang, T. Lu, P. Luo, and L. Shao, "Pyramid vision transformer: A versatile backbone for dense prediction without convolutions," in *Proceedings of the IEEE/CVF international conference on computer vision*, 2021, pp. 568–578.
- [8] B. Dong, W. Wang, D.-P. Fan, J. Li, H. Fu, and L. Shao, "Polyp-pvt: Polyp segmentation with pyramid vision transformers," *arXiv preprint arXiv:2108.06932*, 2021.
- [9] J. Chen, Y. Lu, Q. Yu, X. Luo, E. Adeli, Y. Wang, L. Lu, A. L. Yuille, and Y. Zhou, "Transunet: Transformers make strong encoders for medical image segmentation," *arXiv preprint arXiv:2102.04306*, 2021.
- [10] J. Chen, J. Mei, X. Li, Y. Lu, Q. Yu, Q. Wei, X. Luo, Y. Xie, E. Adeli, Y. Wang *et al.*, "Transunet: Rethinking the u-net architecture design for medical image segmentation through the lens of transformers," *Medical Image Analysis*, vol. 97, p. 103280, 2024.
- [11] H. Cao, Y. Wang, J. Chen, D. Jiang, X. Zhang, Q. Tian, and M. Wang, "Swin-unet: Unet-like pure transformer for medical image segmentation," in *European conference on computer vision*. Springer, 2022, pp. 205–218.
- [12] V. I. Butoi, J. J. G. Ortiz, T. Ma, M. R. Sabuncu, J. Guttag, and A. V. Dalca, "Universeg: Universal medical image segmentation," in *Proceedings of the IEEE/CVF International Conference on Computer Vision*, 2023, pp. 21 438–21 451.
- [13] H. Xiao, L. Li, Q. Liu, X. Zhu, and Q. Zhang, "Transformers in medical image segmentation: A review," *Biomedical Signal Processing and Control*, vol. 84, p. 104791, 2023.
- [14] J. Bernal, F. J. Sánchez, G. Fernández-Esparrach, D. Gil, C. Rodríguez, and F. Vilariño, "Wm-dova maps for accurate polyp highlighting in colonoscopy: Validation vs. saliency maps from physicians," *Computerized medical imaging and graphics*, vol. 43, pp. 99–111, 2015.
- [15] P. Tschandl, C. Rosendahl, and H. Kittler, "The ham10000 dataset, a large collection of multi-source dermatoscopic images of common pigmented skin lesions," *Scientific data*, vol. 5, no. 1, pp. 1–9, 2018.
- [16] N. Codella, V. Rotemberg, P. Tschandl, M. E. Celebi, S. Dusza, D. Gutman, B. Helba, A. Kalloo, K. Liopyris, M. Marchetti *et al.*, "Skin lesion analysis toward melanoma detection 2018: A challenge hosted by the international skin imaging collaboration (isic)," *arXiv preprint arXiv:1902.03368*, 2019.
- [17] D.-P. Fan, G.-P. Ji, T. Zhou, G. Chen, H. Fu, J. Shen, and L. Shao, "Pranet: Parallel reverse attention network for polyp segmentation," in *International conference on medical image computing and computer-assisted intervention*. Springer, 2020, pp. 263–273.
- [18] C.-H. Huang, H.-Y. Wu, and Y.-L. Lin, "Hardnet-mseg: A simple encoder-decoder polyp segmentation neural network that achieves over 0.9 mean dice and 86 fps," *arXiv preprint arXiv:2101.07172*, 2021.
- [19] I. Loshchilov, "Decoupled weight decay regularization," *arXiv preprint arXiv:1711.05101*, 2017.
- [20] W. Wang, E. Xie, X. Li, D.-P. Fan, K. Song, D. Liang, T. Lu, P. Luo, and L. Shao, "Pvt v2: Improved baselines with pyramid vision transformer," *Computational Visual Media*, vol. 8, no. 3, pp. 415–424, 2022.
- [21] Z. Liu, Y. Lin, Y. Cao, H. Hu, Y. Wei, Z. Zhang, S. Lin, and B. Guo, "Swin transformer: Hierarchical vision transformer using shifted windows," in *Proceedings of the IEEE/CVF international conference on computer vision*, 2021, pp. 10 012–10 022.
- [22] J. Wei, S. Wang, and Q. Huang, "F<sup>3</sup>net: fusion, feedback and focus for salient object detection," in *Proceedings of the AAAI conference on artificial intelligence*, vol. 34, no. 07, 2020, pp. 12 321–12 328.
- [23] J. Su, Z. Liu, J. Zhang, V. S. Sheng, Y. Song, Y. Zhu, and Y. Liu, "Dv-net: Accurate liver vessel segmentation via dense connection model with d-bce loss function," *Knowledge-Based Systems*, vol. 232, p. 107471, 2021.
- [24] L. R. Dice, "Measures of the amount of ecologic association between species," *Ecology*, vol. 26, no. 3, pp. 297–302, 1945.
- [25] P. Jaccard, "The distribution of the flora in the alpine zone. 1," *New phytologist*, vol. 11, no. 2, pp. 37–50, 1912.
- [26] A. A. Taha and A. Hanbury, "Metrics for evaluating 3d medical image segmentation: analysis, selection, and tool," *BMC medical imaging*, vol. 15, pp. 1–28, 2015.
- [27] R. Azad, E. K. Aghdam, A. Rauland, Y. Jia, A. H. Avval, A. Bozorgpour, S. Karimijafarbigloo, J. P. Cohen, E. Adeli, and D. Merhof, "Medical image segmentation review: The success of u-net," *arXiv preprint arXiv:2211.14830*, 2022.
- [28] C. Qian, T. Liu, H. Jiang, Z. Wang, P. Wang, M. Guan, and B. Sun, "A detection and segmentation architecture for skin lesion segmentation on dermoscopy images," *arXiv preprint arXiv:1809.03917*, 2018.
- [29] Z. A. Nazi and T. A. Abir, "Automatic skin lesion segmentation and melanoma detection: Transfer learning approach with u-net and dcnn-svm," in *Proceedings of International Joint Conference on Computational Intelligence: IJCCI 2018*. Springer, 2020, pp. 371–381.
- [30] H. Du, J. Y. Seok, D. Ng, N. Yuan, and M. Feng, "Team holidayburned at isic challenge 2018," *Technical report*, 2018.
- [31] Y. Xue, L. Gong, W. Peng, X. Huang, and Y. Zheng, "Automatic skin lesion analysis with deep networks. 2018," 2018.
- [32] N. A. Koohbanani, M. Jahanifar, N. Z. Tajeddin, A. Gooya, and N. M. Rajpoot, "Leveraging transfer learning for segmenting lesions and their attributes in dermoscopy images," *arXiv preprint arXiv:1809.10243*, 2018.